PHYSICAL REVIEW B **91**, 014410 (2015)

Valence-specific magnetization of the charge-ordered multiferroelectric $LuFe_2O_4$ using soft x-ray magnetic circular dichroism under 30 T pulsed high magnetic fields

Yasuo Narumi,[1,*] Tetsuya Nakamura,[2] Kota Saito,[1] Takayuki Morioka,[1] Yukimasa Fukada,[3] Takashi Kambe,[3] Naoshi Ikeda,[3] Yoshinori Kotani,[2] Toyohiko Kinoshita,[2] Koichi Kindo,[4] and Hiroyuki Nojiri[1]

[1]*Institute for Materials Research, Tohoku University, Sendai, Miyagi 980-8577, Japan*

[2]*Japan Synchrotron Radiation Research Institute, SPring-8, Sayo, Hyogo 679-5198, Japan*

[3]*Department of Physics, Okayama University, Okayama 700-8530, Japan*

[4]*The Institute for Solid State Physics, The University of Tokyo, Kashiwa, Chiba 277-8581, Japan*

(Received 9 October 2014; revised manuscript received 15 December 2014; published 12 January 2015)

Soft x-ray magnetic circular dichroism (XMCD) have been measured on the single crystal of the charge-ordered type multiferroelectric material $LuFe_2O_4$. By comparing the XMCD results with the bulk magnetizations, the valence-specific magnetizations (VSMs) of Fe^{2+} and Fe^{3+} ions are obtained. Both Fe^{2+} and Fe^{3+} ions show positive and negative remanent VSMs below the spin ordering temperature $T_{SO} \sim 250$ K, showing the ferrimagnetic long-range ordering directly. Both of the remanent VSMs disappear above the T_{SO} and the field dependencies of the VSMs behave in paramagnetic fashions with convex and concave curvatures. However, the signs of the VSMs of Fe^{2+} and Fe^{3+} remain opposite, nevertheless the system is in a paramagnetic phase. This is direct evidence of the robust antiferromagnetic interaction between Fe^{2+} and Fe^{3+} ions even above the T_{SO}. As temperature increases, furthermore, the opposite VSM of Fe^{3+} is reversed around the three-dimensional charge ordering temperature $T_{CO} \sim 330$ K showing that both net magnetic moments of Fe^{2+} and Fe^{3+} become parallel to the applied magnetic field. Possible correlation between these unusual magnetic behaviors and the ferroelectric properties of $LuFe_2O_4$ is discussed.

DOI: 10.1103/PhysRevB.91.014410 PACS number(s): 75.50.Gg, 75.85.+t, 77.22.−d, 78.20.Ls

I. INTRODUCTION

Multiferroic materials are candidates for next-generation electronic devices, where two order parameters, a magnetization (m) and an electric polarization (p) can be controlled by a magnetic field (B) and a electric field (E), respectively, and vice versa. The discovery of the unique correlation phenomena between the m and the p in the rare earth manganite $TbMnO_3$ [1] prompted intense interests to uncover underlying magnetism as an origin of the dielectric property. The spiral spin magnetic ordering is one of the important mechanisms for multiferroicity in which the inverse Dzyaloshinskii-Moriya (DM) interaction causes a displacement of the oxygen positions resulting in an occurrence of electric polarization [2]. Besides $TbMnO_3$ [1], $CoCr_2O_4$ [3], $CuFeO_2$ [4], $MnWO_4$ [5], etc. have been vigorously studied as so-called *spin-driven ferroelectric materials*. In these systems, understanding of magnetic structures in the ferroelectric states are key issues.

$LuFe_2O_4$ (hereafter abbreviated as LFO) is another class of multiferroic materials, which is named *electronic ferroelectric material* as opposed to *spin-driven ferroelectric material*, because the spontaneous electric polarization appears without any magnetic ordering [6]. LFO is the iron-based mixed valence compound. Both di- (Fe^{2+}) and tri- (Fe^{3+}) valence irons form triangular lattice bilayers stacking along the c axis [7]. Because the formal valence of the Fe ion is 2.5+ in LFO, an equal number of Fe^{2+} and Fe^{3+} coexist on the triangular lattice at low temperatures. The electron and x-ray diffraction experiments [8] clearly revealed the successive phase transition in the charge configuration from two-dimensional charge density wave to three-dimensional (3D) charge ordering (CO) with the wave vector of (1/3, 1/3) in the triangular lattice layers. At about the CO temperature $T_{CO} \sim 330$ K, dielectric anomalies and a spontaneous electric polarization emerge [6]. Moreover, the magnitude of the electric polarization starts to increase again around $T_{SO} = 250$ K, where a ferrimagnetic spin ordering (SO) is realized. Although the magnetoelectric effect is thought to be an inherent nature in $LuFe_2O_4$, the underlying microscopic magnetism, such as an origin of giant magnetic coercivity [9] as well as valence-specific spin structure, are still highly controversial issues [10–14].

In this paper we present the experimental results of magnetic field and temperature dependencies of the magnetic circular dichroism of x-ray absorption spectroscopy (XAS) at the $L_{2,3}$ edge of Fe in LFO. Recently the XMCD measurement has become common as spectroscopic magnetometry. By tuning an incident x-ray energy to the absorption edge of specific elements, the XMCD signal gives element-specific magnetizations. Furthermore, because the resonant energy is dependent on the valence states of the elements, we also obtain valence-specific magnetizations (VSMs). Especially, the XMCD in the soft x-ray region is information directly from magnetically important $3d$ orbitals of transition metal ions, because the L-edge x-ray absorption occurs by a dipole transition from $2p$ to $3d$ shells.

Synchrotron x-ray spectroscopies in pulsed high magnetic fields have been operated in the following hard x-ray beamlines: BL22 of SPring-8 [15] and ID24 of ESRF [16], however, no pulsed high-field experiment in a soft x-ray region has been reported because of several technical difficulties such as ultrahigh vacuum for sample environments and precise current measurement to detect x-ray absorption signals. Although recently the 14 T superconducting magnet has been installed at the soft x-ray beamline of the Diamond Light Source [17], our apparatus is a unique method to investigate

*narumi@imr.tohoku.ac.jp

soft x-ray absorptions in magnetic fields beyond the 14 T and more.

Here we report the VSMs of di and tri valence of Fe ion in LFO in pulsed magnetic fields up to 30 T. The temperature dependencies of the VSM clarify that the short-ranged but robust ferrimagnetism composed of Fe^{2+} and Fe^{3+} ions survive till the three-dimensional charge ordering temperature T_{CO}.

II. EXPERIMENTAL PROCEDURES

The XAS and XMCD measurements have been performed at BL25SU of SPring-8. Right (helicity minus) and left (helicity plus) circularly polarized x rays are produced with the repetition rate of 1 Hz from the twin-helical undulators. The total electron yield method is adopted to record the XAS signal. The XMCD is defined as the difference between the XAS intensities with right circularly polarized x ray (μ_-) and that with left circularly polarized x ray (μ_+). An electromagnet [18] and a pulse magnet [19,20] are used to produce magnetic fields up to 1.9 and 30 T, respectively. High quality single crystals of $LuFe_2O_4$ were grown by a floating zone melting method. A clean surface was obtained by *in situ* cleavages under ultrahigh vacuum better than 5×10^{-7} Pa. The incident beam and the applied magnetic field are normal to the *c* plane, which corresponds to the cleaved plane. Temperature and magnetic field dependencies of the magnetizations of the bulk crystal have been measured in order to confirm the transition temperatures T_{SO} and T_{CO} by a SQUID magnetometer.

Next, we will mention a procedure to record XAS signals in pulsed magnetic fields. Figure 1 are typical time profiles

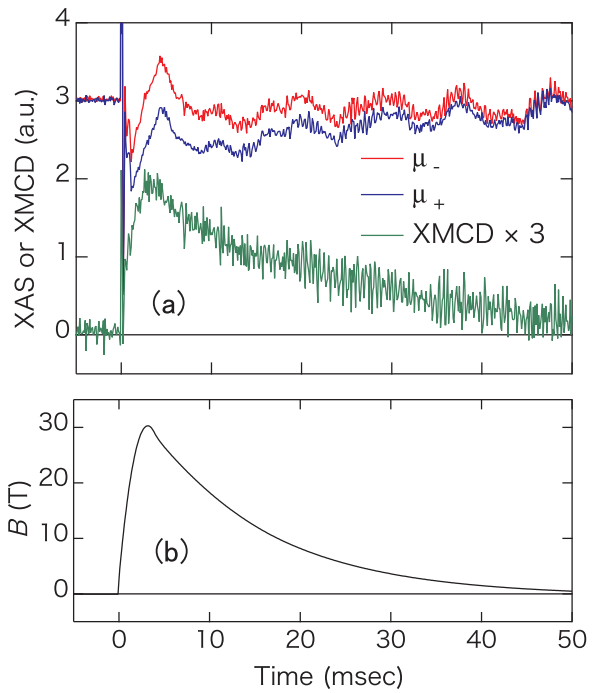

FIG. 1. (Color online) (a) Time profiles of XASs with right (μ_-, red) and left (μ_+, blue) circular polarized x-ray beams and the difference (green) between them corresponding to XMCD. The XMCD is enlarged by a scale factor of three. (b) Time profile of an applied magnetic field up to 30 T.

of original XASs (μ_- and μ_+), XMCD, and an applied pulsed high magnetic field, which are plotted every 0.1 ms. Because we want to measure continuous time variation of XAS, a uniform filling bunch mode is desired. In order to get polarization dependencies of the XASs, we apply at least two pulses of magnetic fields which are synchronized with the right and left circular polarizations of an x ray. Although the original XAS signals contain background noises originating from the applied high magnetic fields as well as XMCD signals, the noises are reproducible very well and XMCD signals change polarity. Therefore, the difference between μ_- and μ_+, namely pure XMCD signal, is hardly influenced at all by applications of high magnetic fields. Although a three-point smoothing is used to make a graph, concretely it takes six pulses (three μ_- and three μ_+) of magnetic fields to get the XMCD data within the present experimental accuracy shown in Fig. 7(d). It is important to note that a sign of the XMCD in the pulsed magnetic field measurement is positive. This is because the propagation vector of the x ray is antiparallel to the direction of the pulsed high magnetic field.

III. RESULTS

Temperature dependence of bulk magnetizations (M_{Total}) in magnetic fields of 0.1 T applied normal to the *c* plane is shown in Fig. 2(a). At $T_{SO} = 250$ K, the magnetization increases steeply with decreasing temperature showing an onset of the spin ordering. In the ZFC (zero field cool), FC (field cool), and TRM (thermal remanent magnetization) curves below T_{SO}, abrupt decreases of M_{Total} around 155 and 235 K are observed. The lower temperature of 155 K is close to the temperature where Christianson *et al.* [10] reported a broadening of the magnetic Bragg peak along with a diffuse component. It suggests that the stacking faults of the antiferromagnetic ordering may reduce the magnetization along the *c* axis. Although the temperature evolution of M_{Total} at $T_{SO} \sim 330$ K is subtle, the inverse magnetic susceptibility shown in Fig. 2(b) has a change of a slope around T_{CO}. A dotted line is a Curie-Weiss fitting from 345 to 400 K. Weiss temperature and effective magnetic moment are obtained to be $\theta = 87.01$ K and $\mu_{eff} = 3.59$. The effective moment is much smaller than 5.41, which is an average of μ_{eff} of Fe^{2+} and Fe^{3+} without taking into account magnetic interactions. This means that the net magnetic moment of Fe is still shortened by antiferromagnetic interactions above T_{CO} as discussed again later. Figure 2(c) represents magnetic field dependencies of M_{Total} after ZFC at 220 and 260 K which are just below and above T_{SO}, respectively. A steep initial rise of M_{Total} is a distinct indication that $LuFe_2O_4$ is in the ferrimagnetic ordered state below T_{SO}. On the other hand, the curvature measured at 260 K intercepts the origin linearly, showing the temperature region above T_{SO} is essentially a paramagnetic phase. The inset is an enlargement of the field dependence of M_{Total}. In general, ferromagnet or ferrimagnet should have a spontaneous magnetization. However, inside the hysteresis loop of *M* of LFO at 220 K, there is a plateau below 0.1 T and the spontaneous magnetization is almost zero. Such behavior also indicates that the weak antiferromagnetic interaction along the *c* axis, which induces the intermediate phase around 155 K, still affects the magnetism of LFO just below T_{SO}. The further

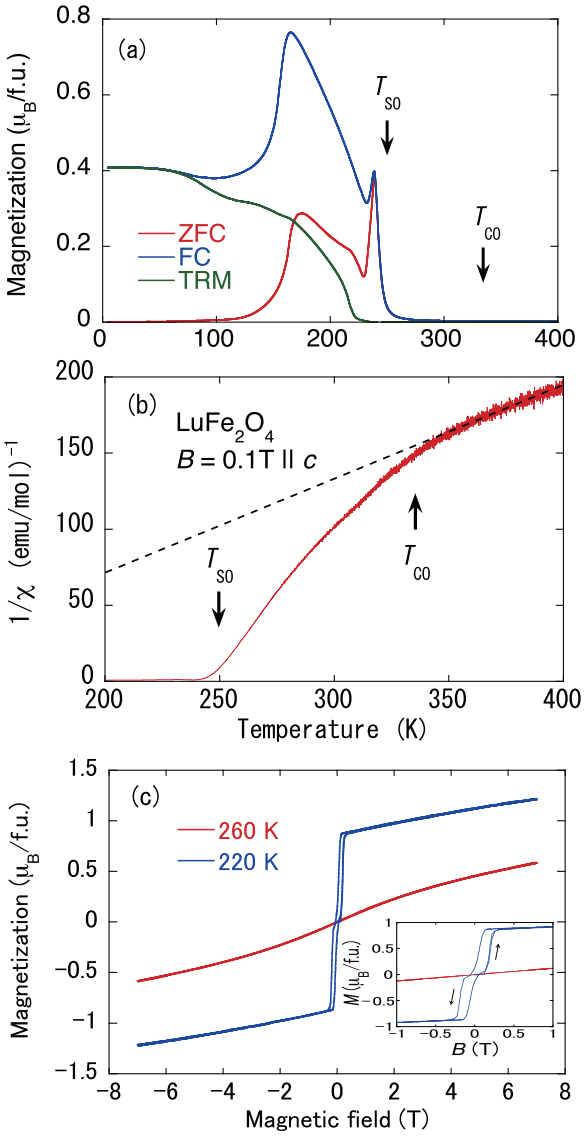

FIG. 2. (Color online) (a) Temperature dependencies of magnetizations (M_{Total}) of $LuFe_2O_4$ when B is along the c axis. ZFC (red), FC (blue), and TRM (green) are abbreviations for data recorded in *zero field cooling*, that in *field cooling*, and *thermal remanent magnetization*. (b) The temperature dependence of the inverse susceptibility from around T_{SO} to T_{CO}. Arrows in (a) and (b) represent transition temperatures of T_{SO} and T_{CO}. (c) Magnetization process is measured at 220 (red) and 260 (blue) K. The inset of (c) is an enlargement around zero magnetic field.

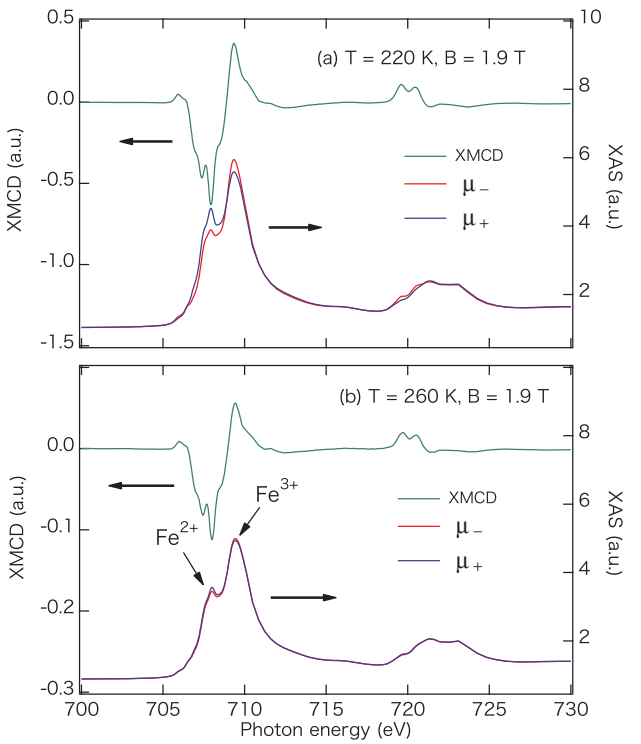

FIG. 3. (Color online) XAS and XMCD measured at $T = 220$ K (a) and $T = 260$ K (b) in steady magnetic fields of 1.9 T. XMCDs are given by $(\mu_-) - (\mu_+)$.

study of these phenomena in low magnetic fields lies outside the scope of this paper.

Figures 3(a) and 3(b) represent the Fe $L_{2,3}$-edge XAS and XMCD measured at temperatures of 220 and 260 K in static magnetic fields of ±1.9 T. Switching of both x-ray helicities and polarities of the magnetic fields is used for XMCD in order to remove extrinsic artifacts. The spectral profiles of XAS at the L_3 edge are characterized by distinct two peaks at 708.0 and 709.3 eV, which correspond to the charge-ordered di- and tri-valence states [14], respectively. The XMCD signals around the di- and tri-valence peaks of XAS take negative and positive signs, respectively. In other words, the net magnetic moment of Fe^{2+} is directed parallel to the applied magnetic field, while that of Fe^{3+} is antiparallel, meaning that an effective antiferromagnetic interaction between the Fe^{2+} and Fe $^{3+}$ sites exists. The ratio of XMCD intensities at the di- and tri-valence peaks is about 1.7, which agrees very well with the result by Ko *et al.* [14]. Interestingly, although the intensities of both XMCDs at 260 K decrease smaller than those at 220 K, the XMCDs are still different in sign even at $T = 260$ K in the paramagnetic phase above T_{SO}.

The peak intensity at each valence of the Fe ion in the XMCD spectra is not necessarily in proportion to the VSM, because the individual XMCD spectra may overlap with each other in general. In order to deconvolute respective XMCD signals from the full XMCD spectra experimentally, we measured the XMCD and XAS of $LuFeCoO_4$ (LFCO) as a reference compound shown in Fig. 4. LFCO is an antiferromagnet with $T_N \sim 90$ K [21]. The measurement of LFCO has been carried out at 110 K which is slightly higher than T_N, because a large XMCD signal and no influence of the magnetic ordering are expected. In the LFCO, half of the Fe sites of LFO are regularly replaced by Co ions which take a valence of 2+ due to electronegativity. This means that the remaining Fe ion in LFCO should take a valence of 3+ to compensate for the charge balance. In Fig. 4(a) we see both Fe and Co $L_{2,3}$-edge absorption peaks in the XAS of LFCO. The XAS peak of the Fe L_3 edge of LFCO is situated at 709.3 eV, which is consistent with the peak on the higher energy side of the Fe L_3 edge of LFO. On the other hand, at the position on the lower energy side of the Fe L_3 edge of LFO, we confirmed the absence of a peak in the XAS of LFCO. As shown in Fig. 4(b),

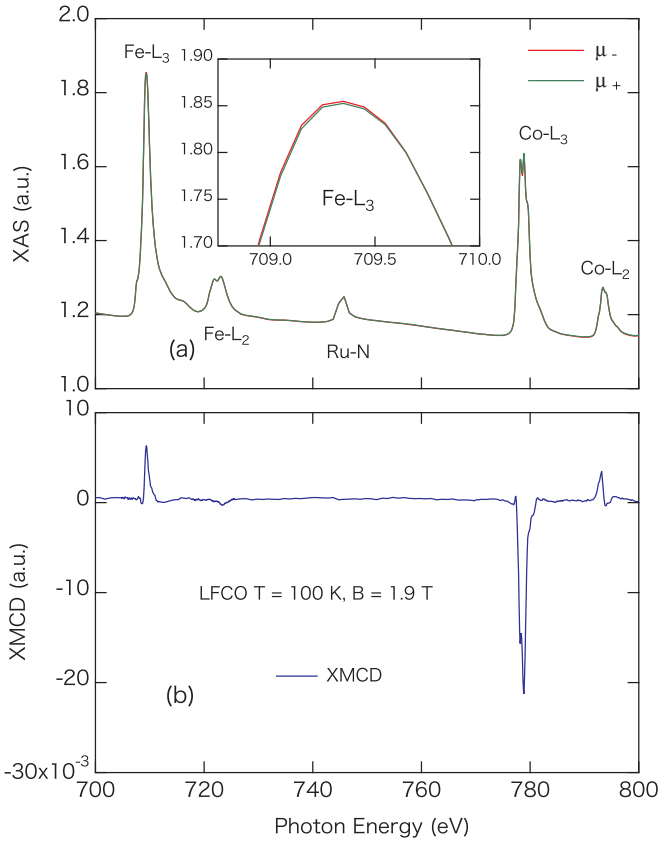

FIG. 4. (Color online) The XAS (a) and XMCD (b) profiles of $LuFeCoO_4$. The inset of (a) is an expansion around the Fe-L_3 peak. There seems to be no difference between μ_- and μ_+, however, there is no doubt that μ_- is slightly larger than μ_+ around Fe-L_3 as shown in the inset and μ_- is smaller than μ_+ around Co-L_3 within our experimental accuracy. It is more pronounced in the XMCD.

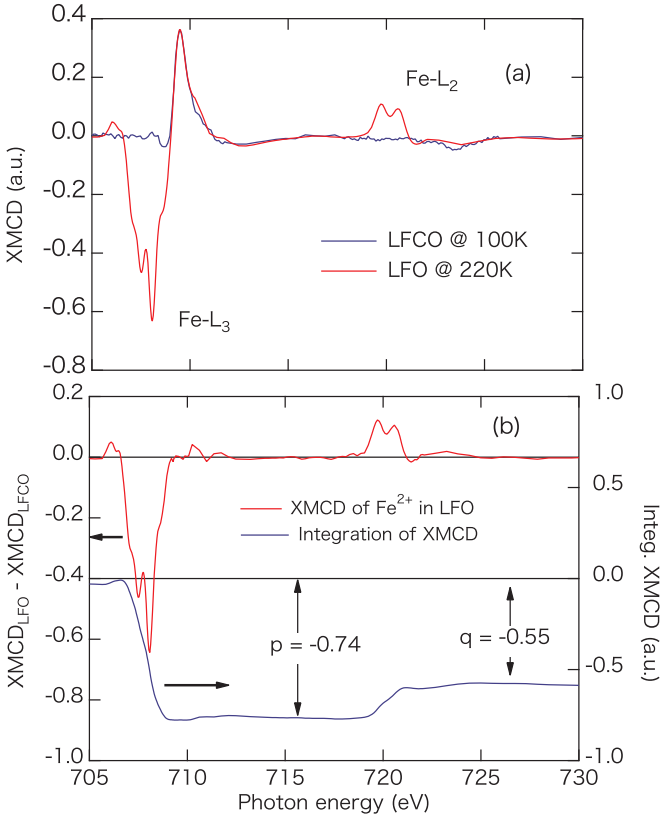

FIG. 5. (Color online) The comparison between the XMCD of LFCO and LFO (a). The absolute value of the XMCD of LFCO is scaled to the XMCD of LFO and the energy of LFCO is shifted by +0.12 eV. By subtracting the XMCD of LFCO from the full XMCD spectra of LFO, the XMCD of Fe^{2+} of LFO is obtained (b). The integration of the XMCD of Fe^{2+} is likewise plotted in the same panel. We obtained $p = -0.74$ and $q = -0.55$.

the XMCD of the Fe L edge is positive and opposite to the XMCD of the Co L edge, implying that the magnetic moments of Fe^{3+} and Co^{2+} in LFCO are antiparallel and parallel to the applied magnetic field, respectively.

Figure 5(a) denotes that the scaled XMCD profile of LFCO is compared with the XMCD of LFO. Satisfactory agreement is achieved only within the energy region of Fe^{3+}, while no contribution from Fe^{3+} is confirmed at the energy of Fe^{2+}. Hence we can regard the XMCD at each peak with the each VSM, independently. By subtracting the XMCD of LFCO from the full XMCD of LFO, we obtain the XMCD of Fe^{2+} in LFO. The Fe^{2+} XMCD and the integration are shown in Fig 5(b). We obtained $p = -0.74$ and $q = -0.55$ by integration of the XMCD in the energy range from the pre-edge to the L_3 edge for p and the pre-edge to the L_2 edge for q. By applying *sum rule* [22,23] to the result, the ratio of the orbital moment (m_o) to spin moments (m_s) is obtained to be $m_o/m_s = 2q/(9p - 6q) = 0.33$. It is noted that the magnetic dipole term is not taken into account. The m_o/m_s of LFO has been determined in the previous reports [14,24,25], where similar $m_o/m_s \sim 0.3$ are obtained by [14,25], while Kuepper *et al.* [24] report $m_o/m_s \sim 0.7$. In any case, they used the whole XMCD spectra including both Fe^{2+} and Fe^{3+} to evaluate the p and q values, on the other hand, our result was obtained from the XMCD spectra of only Fe^{2+} in LFO. Therefore, we directly conclude that the large orbital moment of LFO purely comes from Fe^{2+}. In fact, the ratio of Fe^{3+} in LFCO, which is estimated to be $m_o/m_s = 0.07$ (not shown), is very small, supporting the fact that the orbital moment of Fe^{3+} is almost absent because of the half-filled $3d^5$ orbital and Hund's rule. It seems reasonable to suppose that the Fe^{3+} in LFO also scarcely has orbital moment. These results support that the unquenched orbital moment of Fe^{2+} in LFO could be a possible origin of the giant magnetic coercivity in LFO [9]. The fact that both p and q have the same negative signs implies that the spin moment is parallel to the orbital moment in LFO. There is no contradiction in the condition of more than half electrons ($3d^6$) in Fe^{2+}.

The field dependencies of the valence-specific magnetizations (VSM) at 220 and 260 K are shown in Figs. 6(a) and 6(b). Quantitative analysis of the VSMs M_{Di} and M_{Tri} has been made by comparison between the bulk magnetizations and the XMCD results. Assuming that the spectral shapes of the XMCDs do not change as a function of magnetic field, the field dependencies of the XMCDs at the peak energies of ~708.0 eV for Fe^{2+} and ~709.3 eV for Fe^{3+} (hereafter abbreviated as $XMCD_{Di}$ and $XMCD_{Tri}$) are scaled to the field dependencies of the VSMs as discussed before. The M_{Total} of LFO is given as

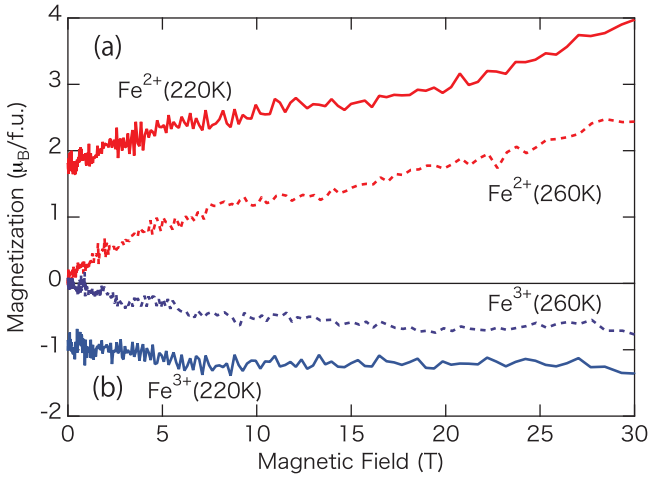

FIG. 6. (Color online) The field dependencies of the valence-specific magnetizations (VSM) of Fe^{2+} (a) and Fe^{3+} (b) at 220 and 260 K derived from the present XMCD study in decreasing magnetic field run. The VSMs are plotted as a red solid line (M_{Di} at 220 K), red dotted line (M_{Di} at 260 K), blue solid line (M_{Tri} at 220 K), and blue dotted line (M_{Tri} at 260 K).

$M_{Total} = M_{Di} + M_{Tri} = \alpha XMCD_{Di} + \beta XMCD_{Tri}$, where the α and β are numerical factors for the $XMCD_{Di}$ and $XMCD_{Tri}$ in the unit of (μ_B/f.u./XMCD). By solving simultaneous equations for the results at 220 and 260 K, the α and β are uniquely determined to be $\alpha = -3.87, \beta = -3.33$. Putting these parameters in the respective XMCD results again, the VSM's are deduced as shown in Fig. 6.

These results have several features observed in both the bulk magnetization and the static field XMCD. The VSMs at 220 K exhibit the following three features: (1) the signal of Fe^{2+} is opposite in sign to that of Fe^{3+}, (2) an extrapolation from high magnetic field to zero is finite, and (3) above 20 T VSMs of Fe^{3+} do not show any field dependence, while VSMs of Fe^{2+} start to increase gradually again. With increasing temperature to 260 K, features 1 and 3 remain unchanged even in the paramagnetic phase, on the other hand, feature 2 fades away. Feature 2, which corresponds to a spontaneous magnetization, is clear evidence showing that LFO is in the long-range-ordered ferrimagnetic state at 220 K and is not in the long-ranged-ordered phase at 260 K. At 260 K, feature 1 and the convex or concave curves of VSMs indicate that effective ferromagnetic interaction within Fe^{2+} ions and antiferromagnetic interaction between Fe^{3+} ions is still effective even above T_{SO}. It is easy to reconfirm that the magnetization of the paramagnet with spins $S = 2$ or $S = 5/2$ without any magnetic interaction should increase almost linearly at the temperature of 260 K. In other words, we may say that the both Fe^{2+} and Fe^{3+} ions form superparamagnetic clusters. From the viewpoint of the crystallography, $LuFe_2O_4$ consists of iron-oxygen based bilayers separated by nonmagnetic Lu layers. Fe-Fe distances are 3.148 Å in the bilayers and 6.291 Å between the bilayers [7]. Therefore, it seems reasonable to suppose that the exchange interactions within the bilayers are dominant. Neutron diffraction experiments [11,26] have reported that the interbilayer magnetic correlation is very weak, because the peak profile obtained using single crystals is not a clear spot, but a rod indexed with (1/3, 1/3, l) in a hexagonal unit cell. The important point to note is that the correlation length along the c axis decreases rapidly on heating above 210 K. It follows from our findings and previous reports that the two-dimensional superparamagnetic state composed of the Fe-O bilayers is realized in the paramagnetic and ferroelectric phase between T_{SO} and T_{CO}. With respect to feature 3, it needs further consideration. Because all Fe^{2+} spins are widely recognized to be aligned along applied magnetic fields, the magnetization process should reach saturation. In contrast to this, the present result suggests a possibility of antiferromagnetic interactions connecting between Fe^{2+} ions. We shall return to this point later.

The next question is how strong the magnetic interaction is between Fe^{2+} and Fe^{3+}. The field dependencies of VSMs M_{Di} and M_{Tri} at $T = 303$, 320, 340, and 380 K are illustrated in Figs. 7(a)–7(d), respectively. The red and blue arrows are schematic representations of net magnetic moments of Fe^{2+} and Fe^{3+} at different temperatures. Below $T = 303$ K, positive and negative field dependencies of the VSMs of Fe^{2+} and Fe^{3+} are observed. However, at $T = 330$ and 340 K, which are close to T_{CO}, the VSM of Fe^{3+} show little field dependence. Finally, both of the VSMs increase as a function of magnetic field at 380 K. It is important to note that the double peaks in the L_3-edge XAS corresponding to the Fe^{2+} and Fe^{3+} charge ordering are clearly visible at 380 K, but on the other hand, the distinct splitting of the spectra in the Mössbauer experiment in [13] merges into one around T_{CO}. This is evidence that the charge ordering of Fe^{2+} and Fe^{3+} above T_{CO} does not melt but is still fluctuating at a faster rate than a few MHz, which is a general hopping rate detected by a Mössbauer spectroscopy.

Figure 8 are temperature dependencies of the VSMs in magnetic fields of 0, 10, and 20 T. The VSM at 0 T, which corresponds to the spontaneous magnetization, is observed only at 220 K. The field induced VSMs at 10 and 20 T obey almost all Curie-Weiss law. However, the VSM of Fe^{3+} intersects zero around 330 K, implying that the net magnetic moment of Fe^{3+} is reversed. The ratio of VSMs of Fe^{2+} and Fe^{3+} is shown in Fig. 8(b). With decreasing temperature from 330 K, the ratio M_{Di}/M_{Tri} converges to -2.4. With increasing temperature above 330 K, the M_{Di}/M_{Tri} also converges to 2.4, although the sign is opposite. This means that the conversion of the direction of the VSM of Fe^{3+} occurs holding the magnetic configuration at each valence. Namely the magnetic moments of Fe^{3+} are not fully polarized even at the temperature above T_{CO}. Considering three $S = 2$ ($\uparrow Fe^{2+}$) spins and three $S = 5/2$ ($\Uparrow Fe^{3+}$) spins in triple formula units in the hexagonal structure, these spins in the ferrimagnetic ordered phase are thought to be arranged in a sequence of $\uparrow\uparrow\uparrow\Downarrow\Uparrow\Downarrow$ along the c axis. Taking into account only the spin magnetic moments based on this model, $M_{Di}/M_{Tri} = (2 + 2 + 2)/(5/2 - 5/2 - 5/2) = -2.4$. The present result seems to agree with the spin configuration of this ferrimagnetic model. In this scenario, however, a contribution of orbital magnetic moments of Fe^{2+} is not taken into account. The present analysis of the XMCD spectrum notes that the orbital magnetic moment of Fe^{2+} is about 33% of the spin magnetic moment. In other words, the total magnetic moment of Fe^{2+} should not have 4 but 5.3 μ_B/Fe^{2+}. Returning to the VSM results at 220 K, the VSM of Fe^{2+} is about

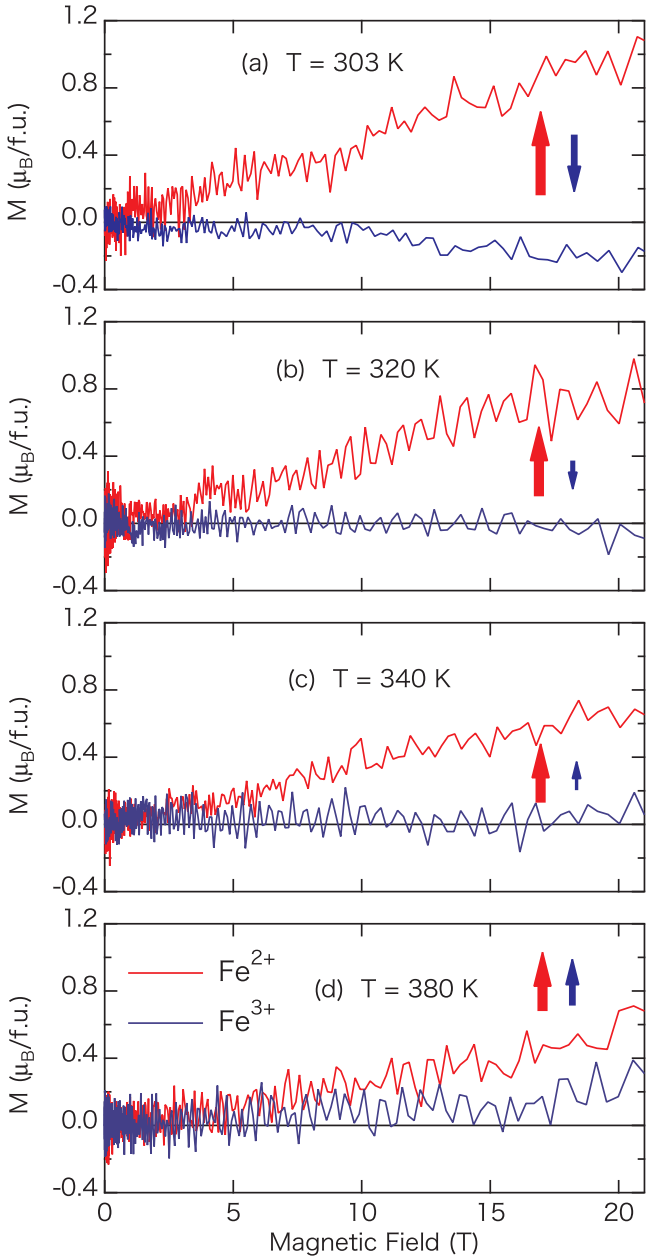

FIG. 7. (Color online) The temperature evolution of the field dependencies of the VSMs of Fe^{2+} and Fe^{3+} at temperatures of 303, 320, 340, and 380 K. Thick arrows are schematic representations of the VSMs for Fe^{2+} (red) and Fe^{3+} (blue).

4 μ_B/f.u. and keeps increasing with increasing magnetic field at 30 T. Because the expected saturation magnetization for Fe^{2+} is 4 μ_B/Fe^{2+} without orbital magnetic moment, the experimental VSM of Fe^{2+} calls for both spin and orbital magnetic moments in order to go beyond 4 μ_B/f.u. On the other hand, the VSM of Fe^{3+} is about 1.3 μ_B/f.u. and shows a little field dependence. Widely recognized spin arrangement of Fe^{3+}: two $S = 5/2$ spins pointing downward and one $S = 5/2$ spin pointing upward, leads to the result that the absolute value of the saturation magnetization is about 1.6 μ_B/Fe^{3+}, which is also larger than the experimental result. In both cases there must be some reasons why VSMs of Fe^{2+} and Fe^{3+} are shorter than the expected values even at 30 T.

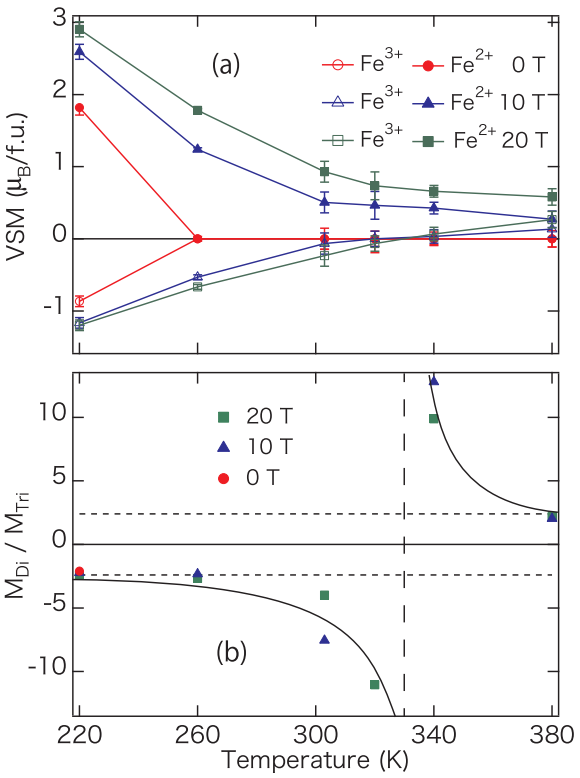

FIG. 8. (Color online) (a) Temperature dependence of the valence-specific magnetizations from 220 to 380 K in applied magnetic fields of 0, 10, and 20 T. (b) Ratios of the VSMs of Fe^{2+} and Fe^{3+}. Two dotted lines are theoretical values of the ratios of VSMs of Fe^{2+} and Fe^{3+} when the spin configurations are up-up-up vs down-down-up and up-up-up vs up-up-down, respectively. Solid lines are guides for the eyes.

Because the magnetic rod of scattering with reduced wave vector (1/3 1/3 l) have been observed [11,26], the stacking pattern of the magnetic planes contains many defects and or randomness. With respect to the in-plane correlation, the magnetic force microscope measurement [11] reveals formations of pancakelike ferrimagnetic domains, which are thought to be a possible origin for robust coercivity. Kambe *et al.* [27] report that the magnetocapacitance effect is clearly related to the evolution of the magnetic domain along the c axis under the magnetic field along the c axis. It is also pointed out that the CO domain boundaries play an important role in the pinning center of the magnetic domain [28]. Furthermore, they insist that the CO domain boundaries are hardly destroyed even by applications of magnetic fields. The bulk magnetization is determined by the volume fraction of the majority and the minority ferrimagnetic domains. The application of the magnetic field can change the volume fraction, however the spins near the pinning center may remain unpolarized, giving rise to the reduction of the saturation magnetization.

IV. DISCUSSION

We have shown temperature and magnetic field dependencies of the valence-specific magnetizations of Fe^{2+} and Fe^{3+} ions in $LuFe_2O_4$ derived from the high-magnetic-field x-ray magnetic circular dichroism measurements. The first

point to notice is that the VSM of Fe^{3+} points in the opposite direction to the VSM of Fe^{2+} above T_{SO} as well as below T_{SO}. In the previous paper by Groot *et al.* [25], they reported this phenomenon with great interest. In the case of a purely paramagnetic system, it is natural that all magnetic moments should point to an applied magnetic field. However, if an antiferromagnetic ordering is restrained by quantum fluctuation or geometrical frustration, even in the paramagnetic phase effective molecular fields induced by an application of a magnetic field make magnetic moments antiparallel with each other. If two different sized magnetic moments exist, longer ones should be directed parallel and shorter ones antiparallel to the magnetic field, resulting in ferrimagnetic moments emerging. In the actual compound $ErCo_2$, the short-range ferrimagnetic alignment of Er and Co ions was observed in the paramagnetic phase and that is called *parimagnetism* [29,30]. In LFO, because exchange interactions through Lu between bilayers should be weaker than those in bilayer, we suggest ferrimagnetic Fe bilayers persist above T_{SO} with strong two-dimensional magnetic correlations.

Even more important is that the VSM of Fe^{3+} flips over around T_{CO}. For a phenomenological discussion we would like to introduce a $S = 1$ and $s = 1/2$ ferrimagnetic dimer as the most simple ferrimagnetic system. LFO is expected to have many kinds of exchange interactions between Fe ions in reality [31], while the dimer has the only one exchange interaction and the thermodynamic variable of the dimer can be calculated exactly. Because the ferrimagnetic dimer does not show any long-range order, namely paramagnet, the dimer can be regarded as the simplified model of LFO above T_{SO} to discuss the paramagnetic temperature dependence of the sublattice magnetizations of LFO. Here we would like to discuss generality of the zero crossing of the VSM around T_{CO}. According to the calculation well below the critical magnetic field, where all spins becomes induced ferromagnetic, we know that the sublattice magnetization of $S = 1$ always points to the magnetic field direction, while at some critical temperature the sublattice magnetization of $S = 1/2$ changes smoothly from antiparallel alignment to a parallel one with temperature increasing. Although this is not a phase transition but a crossover, the temperature corresponds to a characteristic energy region where a magnetic correlation and a thermal fluctuation compete with each other. The important point to note is that the crossover can occur in a paramagnetic system where strong magnetic correlations persist and a long-range magnetic ordering is strongly suppressed. In LFO, the geometrical frustration and the dimensionality of the triangular lattice in the Fe bilayer cause the suppression of the 3D magnetic ordering.

The question arises as to whether this magnetic crossover assists the occurrence of the charge ordering (CO) and the emerging of the ferroelectric polarization in LFO. The theory by Nagano *et al.* [32] concludes that the CO is reinforced by the SO where the entropy gain derived from the spin frustration is important. In the intermediate temperature range from T_{CO} to T_{SO}, the magnetic correlation is not three-dimensionally long range, but the intrabilayer exchange interactions are strong enough to form the two-dimensional short-range network in LFO. In other words, a two-dimensional spin ordering already occurs at T_{CO} and a subsequent three-dimensional one occurs at T_{SO} on cooling. What is important is that the local spin alignments in both cases are the same. It seems reasonable to suppose that the CO occurs not at T_{SO} but at T_{CO} thanks to the two-dimensional SO.

V. SUMMARY

We conducted x-ray magnetic circular dichroism measurements at the $L_{2,3}$ edge of Fe in $LuFe_2O_4$ under pulsed high magnetic field up to 30 T. Below T_{SO}, a large orbital moment coming solely from Fe^{2+} was determined. This is a possible origin of the Ising anisotropy and the giant magnetic coercivity in LFO. Above T_{SO} the field dependence of the VSM of Fe^{2+} and Fe^{3+} behave in paramagnetic manners with convex and concave curvature. However, the sign of the VSMs remain opposite to each other as well as below T_{SO}, evidencing the robust antiferromagnetic interaction between Fe^{2+} and Fe^{3+} ions even above T_{SO}. The negative VSM of Fe^{3+} is reversed to positive around T_{CO}, indicating the importance of the spin-charge coupling in the bilayer with considerable two-dimensional short-range spin correlation.

ACKNOWLEDGMENTS

The authors would like to express many thanks to S. Ishihara and H. Nakano for their valuable discussions and T. Hirono, M. Higashiyama, and N. Tsuji for their technical supports. This work has been carried out with the approval of the SPring-8 Program Advisory Committee (Proposals No. 2011A1512, No. 2011B1079, No. 2012A1429, No. 2013A1255, and No. 2013A1909). This work was supported by JSPS KAKENHI Grants No. 21340107, No. 23340094, and No. 23224009 and is partly supported by JASRI's GIGNO project and Shimadzu Science Foundation.

[1] T. Kimura, T. Goto, H. Shintani, K. Ishizaka, T. Arima, and Y. Tokura, Nature (London) **426**, 55 (2003).

[2] H. Katsura, N. Nagaosa, and A. V. Balatsky, Phys. Rev. Lett. **95**, 057205 (2005).

[3] Y. Yamasaki, S. Miyasaka, Y. Kaneko, J.-P. He, T. Arima, and Y. Tokura, Phys. Rev. Lett. **96**, 207204 (2006).

[4] T. Kimura, J. C. Lashley, and A. P. Ramirez, Phys. Rev. B **73**, 220401(R) (2006).

[5] K. Taniguchi, N. Abe, T. Takenobu, Y. Iwasa, and T. Arima, Phys. Rev. Lett. **97**, 097203 (2006).

[6] N. Ikeda, H. Ohsumi, K. Ohwada, K. Ishii, T. Inami, K. Kakurai, Y. Murakami, K. Yoshii, S. Mori, Y. Horibe, and H. Kitô, Nature (London) **436**, 1136 (2005).

[7] M. Isobe, N. Kimizuka, J. Iida, and S. Takewaka, Acta Crystallogr. **C46**, 1917 (1990).

[8] Y. Yamada, S. Nohdo, and N. Ikeda, J. Phys. Soc. Jpn. **66**, 3733 (1997).

[9] J. Iida, Y. Nakagawa, S. Takewaka, and N. Kimizuka, J. Phys. Soc. Jpn. **56**, 3746 (1987).
[10] A. D. Christianson, M. D. Lumsden, M. Angst, Z. Yamani, W. Tian, R. Jin, E. A. Payzant, S. E. Nagler, B. C. Sales, and D. Mandrus, Phys. Rev. Lett. **100**, 107601 (2008).
[11] W. Wu, V. Kiryukhin, H.-J. Noh, K.-T. Ko, J.-H. Park, W. Ratcliff II, P. A. Sharma, N. Harrison, Y. J. Choi, Y. Horibe, S. Lee, S. Park, H. T. Yi, C. L. Zhang, and S.-W. Cheong, Phys. Rev. Lett. **101**, 137203 (2008).
[12] M. Angst, R. P. Hermann, A. D. Christianson, M. D. Lumsden, C. Lee, M.-H. Whangbo, J.-W. Kim, P. J. Ryan, S. E. Nagler, W. Tian, R. Jin, B. C. Sales, and D. Mandrus, Phys. Rev. Lett. **101**, 227601 (2008).
[13] X. S. Xu, M. Angst, T. V. Brinzari, R. P. Hermann, J. L. Musfeldt, A. D. Christianson, D. Mandrus, B. C. Sales, S. McGill, J.-W. Kim, and Z. Islam, Phys. Rev. Lett. **101**, 227602 (2008).
[14] K.-T. Ko, H.-J. Noh, J.-Y. Kim, B.-G. Park, J.-H. Park, A. Tanaka, S. B. Kim, C. L. Zhang, and S.-W. Cheong, Phys. Rev. Lett. **103**, 207202 (2009).
[15] Y. H. Matsuda, Y. Murata, T. Inami, K. Ohwada, H. Nojiri, K. Ohoyama, N. Katoh, Y. Murakami, F. Iga, T. Takabatake, A. Mitsuda, and H. Wada, J. Phys.: Conf. Ser. **51**, 490 (2006).
[16] O. Mathon, P. van der Linden, T. Neisius, M. Sikora, J. M. Michalik, C. Ponchut, J. M. De Teresa, and S. Pascarelli, J. Synch. Rad. **14**, 409 (2007).
[17] G. B. G. Stenning, G. J. Bowden, S. A. Gregory, P. A. J. de Groot, G. van der Laan, L. R. Shelford, P. Bencok, P. Steadman, A. N. Dobrynin, and T. Hesjedal, Phys. Rev. B **86**, 174420 (2012).
[18] T. Nakamura, T. Muro, F. Z. Guo. T. Matsushita, T. Wakita, T. Hirono, Y. Takeuchi, and K. Kobayashi, J. Electron. Spectrosc. Relat. Phenom. **144-147**, 1035 (2005).
[19] T. Nakamura, Y. Narumi, T. Hirono, M. Hayashi, K. Kodama, M. Tsunoda, S. Isogami, H. Takahashi, T. Kinoshita, K. Kindo, and H. Nojiri, Appl. Phys. Express **4**, 066602 (2011).
[20] Y. Narumi, T. Nakamura, T. Kinoshita, Y. H. Matsuda, and H. Nojiri, Synch. Rad. News **25**, 12 (2012).
[21] K. Yoshii, N. Ikeda, Y. Matsuo, Y. Horibe, and S. Mori, Phys. Rev. B **76**, 024423 (2007).
[22] C. T. Chen, Y. U. Idzerda, H.-J. Lin, N. V. Smith, G. Meigs, E. Chaban, G. H. Ho, E. Pellegrin, and F. Sette, Phys. Rev. Lett. **75**, 152 (1995).
[23] B. T. Thole, P. Carra, F. Sette, and G. van der Laan, Phys. Rev. Lett. **68**, 1943 (1992).
[24] K. Kuepper. M. Raekers, C. Taubitz, M. Prinz, C. Derks, M. Neumann, A. V. Postnikov. F. M. F. de Groot, C. Piamonteze, D. Prabhakaran, and S. J. Blundell, Phys. Rev. B **80**, 220409(R) (2009).
[25] J. de Groot, T. Mueller, R. A. Rosenberg, D. J. Keavney, Z. Islam, J.-W. Kim, and M. Angst, Phys. Rev. Lett. **108**, 187601 (2012).
[26] J. Iida, M. Tanaka, Y. Nakagawa, S. Funahashi, N. Kimizuka, and S. Takewaka, J. Phys. Soc. Jpn. **62**, 1723 (1993).
[27] T. Kambe, Y. Fukada, J. Kano, T. Nagata, H. Okazaki, T. Yokoya, S. Wakimoto, K. Kakurai, and N. Ikeda, Phys. Rev. Lett. **110**, 117602 (2013).
[28] S. Park, Y. Horibe, Y. J. Choi, C. L. Zhang, S.-W. Cheong, and W. Wu, Phys. Rev. B **79**, 180401(R) (2009).
[29] J. Herrero-Albillos, F. Bartolomé, L. M. García, A. Young, T. Funk, J. Campo, and G. J. Cuello, J. Magn. Magn. Mater. **310**, 1645 (2007).
[30] J. Herrero-Albillos, F. Bartolomé, L. M. García, A. Young, T. Funk, J. Campo, and G. J. Cuello, Phys. Rev. B **76**, 094409 (2007).
[31] H. J. Xiang, E. J. Kan, S. H. Wei, M. H. Whangbo, and J. Yang, Phys. Rev. B **80**, 132408 (2009).
[32] A. Nagano, M. Naka, J. Nasu, and S. Ishihara, Phys. Rev. Lett. **99**, 217202 (2007).